Multi-Objective Optimization Based on Unsteady Analysis Considering the Efficiency and Radial Force of a Single-Channel Pump for Wastewater Treatment

Jin-Hyuk Kim[1,2]*, Bo-Min Cho[1,2], Young-Seok Choi[1,2], Kyoung-Yong Lee[1]

ISROMAC 2016

International Symposium on Transport Phenomena and Dynamics of Rotating Machinery

Hawaii, Honolulu

April 10-15, 2016

Abstract

A multidisciplinary optimization was conducted to simultaneously improve the efficiency and reduce the radial force of a single-channel pump for wastewater treatment. A hybrid multi-objective evolutionary algorithm was coupled with a surrogate model to optimize the geometry of the single-channel pump volute. Steady and unsteady Reynolds-averaged Navier-Stokes equations with a shear stress transport turbulence model were discretized using finite volume approximations and were then solved on tetrahedral grids to analyze the flow in the single-channel pump. The three objective functions represented the total efficiency, the sweep area of the radial force during one revolution, and the distance of the mass center of sweep area from the origin while the two design variables were related to the cross-sectional area of the internal flow of the volute. Latin hypercube sampling was employed to generate twelve design points within the design space, and response surface approximation models were constructed as surrogate models for the objectives based on the values of the objective function at the given design points. A fast non-dominated sorting genetic algorithm for local search was coupled with the surrogate models to determine the global Pareto-optimal solutions. The trade-off between the objectives was determined and was described in terms of the Pareto-optimal solutions. The results of the multi-objective optimization showed that the optimum design simultaneously improved the efficiency and reduced the radial force relative to those of the reference design.

Keywords

Single-channel pump, efficiency, radial force, sweep area, unsteady analysis, optimization.

[1] *Thermal & Fluid System R&D Group, Korea Institute of Industrial Technology, Cheonan, Republic of Korea*

[2] *Advanced Energy & Technology, University of Science and Technology, Daejeon, Republic of Korea*

*__Corresponding author__: jinhyuk@kitech.re.kr

INTRODUCTION

The most common cause for a fault in a submerged pump for wastewater treatment is due to waste clogging. Therefore, this type of pump requires unique design features to prevent a loss in performance due to waste clogging, damage, failure, and so on. Recently, computational fluid dynamics (CFD) and computing power systems have been used to actively investigate various types of flow-path-securing pumps to prevent such problems.

A single-channel pump is a representative case of flow-path-securing pumps, and it has different design features that are unlike those for general pumps that are pressurized by blades. The impeller of a single-channel pump has a free annulus passage without blades, and the contents are blown only by the centrifugal force generated from the rotating passage [1]. Thus, a single-channel pump is robust against failure and damage due to waste clogging.

As a result, demand for single-channel pumps is rapidly growing, and the hydraulic performance of the pump should be improved by undertaking more advanced studies. Nevertheless, only a few studies been presented on the concepts and patents related to single-channel pumps [1-3]. To the best of the author's knowledge, this lack of studies is due to difficulty in establishing a design methodology, manufacturing, and, especially, solving the balancing problem related to the vibration of single-channel pumps rather than for general blade pumps. In fact, the mass distribution of a single-channel impeller is not rotationally symmetric, so the resulting mechanical imbalance needs to be addressed [4].

Over the past several years, there has been growing interest in the dynamic effect of the impeller-volute interaction in centrifugal pumps. For instance, Gonzalez et al. [5] conducted an unsteady numerical analysis and an experimental test to demonstrate the dynamic interaction between the flow at the impeller exit and the volute tongue. They also investigated the static and dynamic effects of the flow in a vaneless volute centrifugal pump with two different impellers [6]. Baun et al. [7] investigated the effect that the relative position of the impeller to the volute had on the hydraulic performance and radial impeller force characteristics in a circular volute casing pump. Kurokawa et al. carried out an experimental study to investigate the flow characteristics in a double volute in order to balance the radial thrust in centrifugal pumps [8]. Wei et al. [9] conducted numerical and experimental studies on the hydraulic performance and radial force of a single-stage pump with diffuse vanes with different outlet diameters, and Kaupert and Staubli [10] performed an experimental

investigation on the unsteady pressure field in a high specific speed centrifugal pump impeller. Baun and Flack [11] experimentally analyzed the effects that volute design and the number of impeller blades had on the radial impeller forces and hydraulic performance. Finally, Alemi et al. investigated the effects of the volute geometry on the head, efficiency, and radial force of a low specific speed centrifugal pump under design and off-design conditions [12].

On the other hand, practical turbomachinery designs are generally accompanied by a multitude of problems, and the simultaneous optimization of multiple objectives related to each problem is necessary. Deb [13] developed a fast non-dominated sorting genetic algorithm (NSGA-II) that generates a Pareto-optimal solution (POS) using an evolutionary algorithm, and this algorithm has been employed for multiple optimization problems in order to improve the performance of various turbomachines.

For example, Kim et al. [14] optimized the aerodynamic and aeroacoustic performance of an axial-flow fan using a NSGA-II algorithm combined with a surrogate model based on three-dimensional unsteady Reynolds-averaged Navier-Stokes (RANS) and Ffowcs Williams-Hawkings equations. To improve the multiple aerodynamic performance of an axial compressor, Wang et al. [15] applied a multiple genetic algorithm combined with NSGA-II and a neural network model. Kim et al. [16] maximized the efficiency and turbine output of a counter-rotating pump-turbine unit via shape optimization based on NSGA-II in conjunction with RANS analysis. Okasuz and Akmandor optimized the aerodynamic design by using a novel multi-level genetic algorithm to maximize the adiabatic efficiency and torque of an axial turbine blade [17]. Thus, multiple optimization strategies based on NSGA-II have been proven to be effective in improving the performances of various turbomachines.

As previously mentioned, many numerical and experimental studies have been conducted thus far on hydraulic performance and radial force of various types of centrifugal pumps, but no attempt has yet been made to systematically optimize the design of a single-channel pump by simultaneously considering the efficiency and radial force via steady and unsteady analyses. To this end, this work presents a multidisciplinary optimization procedure to design a single-channel pump by using three-dimensional steady and unsteady RANS equations. Multi-objective optimization was carried out to simultaneously improve the efficiency and reduce the radial force using a hybrid multi-objective evolutionary algorithm (MOEA) [13, 18] coupled with a response surface approximation (RSA) [19] surrogate model with two design variables related to the cross-sectional area of the internal flow of the volute.

The goals of this work are the following. First, to optimize the volute geometry in order to simultaneously improve the efficiency and reduce the radial force of a single-channel pump by using the proposed design optimization method. Second, to understand the trade-off in the three objective functions with respect to changes in the design variables. Finally, to provide guidelines for optimum volute design by considering the impeller-volute interaction.

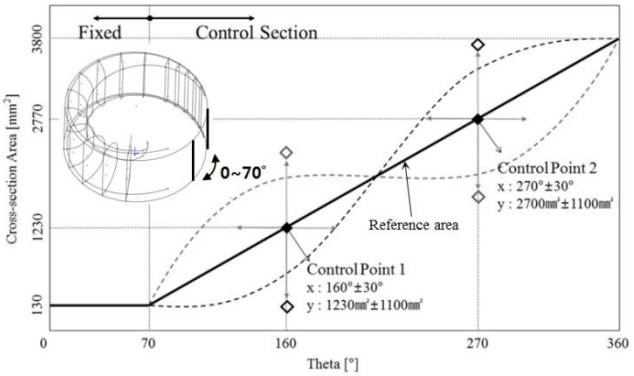

Figure 1. Cross-sectional area showing the distribution of the internal flow of the impeller

Table 1. Design specifications of the single-channel pump impeller

Design volume flow rate, m^3/h	85
Rotational speed, r/min	1,760
Total head, m	10
Efficiency, %	85.24
Diameter of impeller, mm	190

SINGLE-CHANNEL PUMP MODEL

The single-channel pump impeller for wastewater treatment used in this work was initially designed according to the Stepanoff theory from a previous study [20], as shown in Fig. 1. The volumetric flow rate and the total head at the design point of the reference pump impeller are 85 m^3/h and 10 m, respectively, with an efficiency of 85.24%. The additional design specifications are listed in Table 1.

In this work, the reference volute was also designed according to Stepanoff theory. Since Stepanoff theory generally minimizes the flow loss from flow-speed differences by increasing the cross-sectional area of the internal flow at a fixed rate according to the theta angle position, it is especially useful to the volute design. Hence, the distribution in the cross-sectional area of the internal flow changed proportionally along the theta angle position in order to maintain a constant flow velocity in the volute. Fig. 2 shows the distribution of the cross-sectional area of the internal flow of the volute generated from Stepanoff theory.

When the cross-sectional area distribution of the internal flow is determined according to the theta angle, the shape of the area should be defined. In this work, the authors invented a novel design method for the cross section of the high-efficiency single-channel pump volute as follows (Fig. 3).

Given A_t

$$A_t = A_1+A_2+2A_3 \quad (1)$$

$$H = 0.01 \times A_t(@360^\circ),$$

where H is fixed along theta angle (2)

$$R = \text{theta}(^{\circ}) \times C,$$

where $C = 0.1 \times H/89.5$ (expansion coefficient) (3)

$$A_2 = R \times L_2, \text{ where } L_2 = H - 2R \quad (4)$$

$$A_3 = \pi R^2/4 \quad (5)$$

$$A_1 = A_t - A_2 - 2A_3 \quad (6)$$

$$A_{1=} L_1 H \quad (7)$$

Apparently, the maximum cross-sectional area at a theta angle of 360˚ generated from the Stepanoff theory is relatively narrow when compared to the inlet area of the impeller in order to smoothly pass the waste solid. Therefore, the distribution in the cross-sectional area was redesigned by changing the maximum cross-sectional area according to that generated from the Stepanoff theory, as shown in Fig. 2. Here, the changed cross-section area distribution was normalized to the maximum value generated using Stepanoff theory.

Fig. 4 shows the results for the head and the efficiency with the variation in the distribution in the cross-sectional area by the CFD result. As shown in Fig. 4, as the maximum cross-sectional area increases, the head and efficiency are almost similar when compared to that designed using Stepanoff theory. As a result, the distribution in the cross-sectional area with 1.2 times the maximum of that obtained using Stepanoff theory when considering the cross-sectional area of the impeller inlet was finally selected as the reference volute model. Meanwhile, the cross-sectional area of the volute exit was also designed by considering the impeller inlet and the maximum cross-sectional areas.

Therefore, the total head and hydraulic efficiency for the reference single-channel pump model are 9.41 m and 81.06%, respectively, at the design point.

STEADY AND UNSTEADY ANALYSES

In the computational domain, the internal flow field was analyzed by solving three-dimensional steady and unsteady incompressible RANS equations with a shear-stress transport (SST) turbulence model by using a finite-volume solver. The commercial CFD code ANSYS CFX 14.5 was used to this and [21], the three-dimensional model for the single-channel pump impeller and the volute was created using Solidworks 2015, and ICEM-CFD was applied to generate the computational meshes for the pump impeller and the volute. The numerical analysis was carried out with boundary conditions, solving and post-processing of the results conducted using ANSYS CFX-Pre, CFX-Solver and CFX-Post, respectively.

For the turbulence closure model, the k-ω-based SST model [22] was employed to make an accurate prediction of the flow separation under an adverse pressure gradient [23]. In this model, k-ω and k-ε models applied in the near-wall region and in the bulk domain, respectively, and a blending function ensures smooth transitions between these two

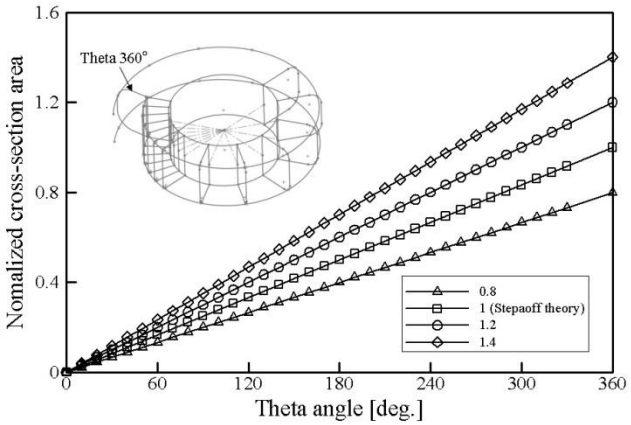

Figure 2. Distribution of the cross-sectional area of the internal flow of the volute

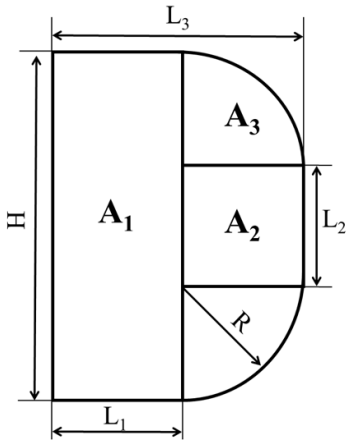

Figure 3. Definition of the cross-sectional area of the volute

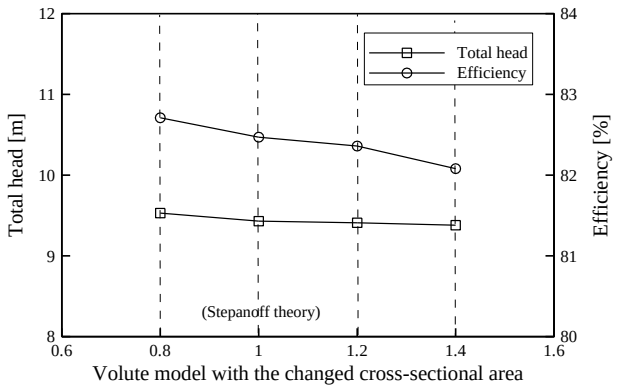

Figure 4. Results for the head and efficiency with the variation in the distribution of the cross-sectional area

models. The accuracy of the numerical analyses of turbulent flows generally depends heavily on treating the wall shear stress. In this work, the near-wall grid resolution was adjusted to maintain y+ ≤ 2 to accurately capture the wall shear stress and to implement a low-Reynolds-number SST model [21].

As shown in Fig. 5, the entire inside domain of the single-channel pump was considered as the computational domain for the numerical analysis. This computational domain namely included a single-channel rotating impeller and volute domains.

Water was considered as the working fluid, and the total pressure and designed mass flow rate were set to the inlet and outlet of the computational domain, respectively. The solid surfaces in the computational domain were considered to be hydraulically smooth under adiabatic and no-slip conditions. As shown in Fig. 5, the wall condition did not exhibit an overlap region between the impeller and volute. The Stage average and Transient-Rotor-Stator methods were respectively applied to connect the interface between the rotating impeller and the volute domains in the steady and unsteady analyses [21].

A tetrahedral grid system was constructed in the computational domain with a prism mesh near the surfaces, as shown in Fig. 5. The rotating impeller and the volute domains were each constructed using approximately 1,300,000 and 1,200,000 grid points. Therefore, the total optimum grid system selected using the grid independency test has approximately 2,500,000 grid points, as previously reported [20].

The convergence criteria in a steady computation consist of the root-mean-square (RMS) values of the residuals of the governing equations, which were set to less than 10^{-5} for all equations. The physical time scale was set to $1/\omega$, where ω is the angular velocity of the impeller. The computations were carried out using an Intel Xeon CPU with a clock speed of 2.70 GHz, and the converged solutions were obtained after 1,000 iterations with a computational time of approximately 4 hrs.

The results of the steady RANS analysis were used in the unsteady RANS analysis to obtain the characteristics of the radial force sources in the region of the exit surface of the impeller according to the impeller-volute interaction in the single-channel pump. In an unsteady computation, the time step and the coefficient loop for the time scale control were set to 0.000947 s and 3 times, respectively. The solutions were obtained after 180 iterations with an unsteady total time duration of 0.1704775 s (five revolutions), and the computational time for the unsteady calculation was approximately 8 hrs.

OPTIMIZATION TECHNIQUE

The purpose of the current multi-objective optimization was to simultaneously improve the hydraulic efficiency and reduce the radial force sources due to the impeller-volute interaction in the single-channel pump. Here, one of three objective functions, the hydraulic efficiency, is defined as follows.

$$\eta = \frac{\rho g H Q}{P} \tag{8}$$

where, ρ, g, H, Q, and P represent the density, acceleration due to gravity, total head, volume flow rate, and power, respectively.

The other objective functions related to the sources of the radial force are defined as the sweep area of the radial force during one revolution and the distance of the mass center of the sweep area from the origin, as follows.

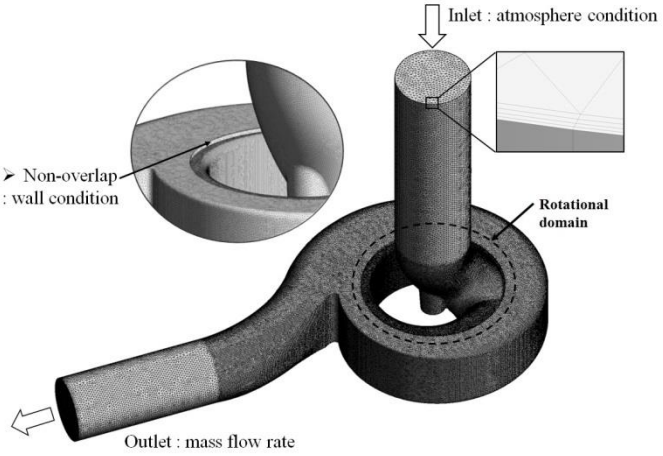

Figure 5. Computational domain and grids

$$A_s = \frac{1}{2}\sum_{i=0}^{n-1}(x_i y_{i+1} - x_{i+1} y_i) \tag{9}$$

where, A_s is the signed area of the polygon as the sweep area of the radial force during one revolution. The centroid of a non-self-intersecting closed polygon defined by n vertices (x_0, y_0), (x_1, y_1), ..., (x_{n-1}, y_{n-1}) is defined as the point (C_x, C_y) as follows.

$$C_x = \frac{1}{6A_s}\sum_{i=0}^{n-1}(x_i + x_{i+1})(x_i y_{i+1} - x_{i+1} y_i) \tag{10}$$

$$C_y = \frac{1}{6A_s}\sum_{i=0}^{n-1}(y_i + y_{i+1})(x_i y_{i+1} - x_{i+1} y_i) \tag{11}$$

In these formulas, the vertices are assumed to be numbered in the order of their occurrence along the perimeter of the polygon. Therefore, the distance of the mass center of the sweep area from the origin is finally defined as follows.

$$D_s = \sqrt{{C_x}^2 + {C_y}^2} \tag{12}$$

In this work, the two objective functions given above are related to the radial force sources and were integrated using the weightng factor to express one objective function. Here, the weighting factor was given equivalently as 0.5.

$$f_{radial} = 0.5A_s + 0.5D_s \tag{13}$$

Thus, η and f_{radial} are expected to be simultaneously improved and reduced by carrying out the multi-objective optimization.

In this work, the geometric parameters related to the

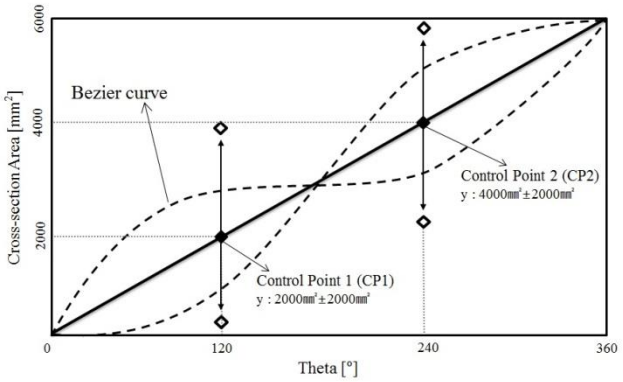

Figure 6. Definition of the design variables

internal flow through the cross-sectional area of the volute were selected as the design variables to simultaneously optimize the hydraulic efficiency and the radial force sources of the single-channel pump for wastewater treatment. The distribution of the cross-sectional area of the internal flow of the volute can change smoothly by adjusting the control points represented by a third-order Bezier-curve, as shown in Fig. 6. Hence, the variation in the y-axes for only two control points (CP1, CP2) was selected for the design variables to obtain the most sensitive results for the curve variation among the control points [24]. Figure 6 shows the defined design variables and their ranges. When the volute optimization is processed with these variables, the optimized pump impeller that maximizes the total efficiency according to the two design variables by using a radial basis neural network surrogate model from the previous work [26] is applied here.

For multi-objective optimization, the RSA surrogate models were employed and constructed to approximate the objective functions based on the values calculated at twelve design points generated in the design space using Latin hypercube sampling (LHS) [25]. In the present work, RSA was employed as the surrogate model to predict the objective function values in the design space. Since RSA functionally expresses the association between the design variables and the response functions, the constructed response of a second-order polynomial RSA can be represented as follows.

$$f(x) = \beta_0 + \sum_{j=1}^{N} \beta_j x_j + \sum_{j=1}^{N} \beta_{jj} x_j^2 + \sum \sum_{i \neq j}^{N} \beta_{ij} x_i x_j \qquad (14)$$

where, β, N, and x are the regression analysis coefficient, the number of design variables, and a set of design variables, respectively. Here, the number of regression analysis coefficients (β_0, β_i, etc.) is $(N+1)\times(N+2)/2$.

A hybrid MOEA coupled with a surrogate model was employed to obtain the global POSs. The approximate POSs were obtained through real-coded fast and elitist NSGA-II code using the evolutionary algorithm for the objective functions in this work. Here, "real-coded" refers to crossovers and mutations being conducted in real space to obtain a response from the NSGA-II code. Then, the POSs were refined by searching for a local optimal solution for each objective function over all NSGA-II derived optimal solutions using sequential quadratic programming (SQP) [26] with NSGA-II solutions as the initial guesses. For the present work, the two approaches that were used are normally used to perform a local search [18]. In the first approach, all objective functions were combined into a single composite objective function, and the optimum models were then determined. In the second approach, one objective function is optimized by treating the others as equality constraints, and the process is then repeated for all objective functions. Here, the first objective function was optimized, and the second objective function was fixed. Local search was then repeated for the second objective function by keeping the first objective function fixed, and this process can produce two new sets of optimal solutions that are then merged with the NSGA-II solutions. The dominant solutions were discarded from these optimal solutions, and duplicate solutions were then removed to produce the global POSs. A local search was subsequently carried out to improve the quality of the POSs. The effectiveness of this optimization algorithm has been demonstrated in previous studies [27~29], and it has become a very practical tool to solve multiple problems for various turbimachinery designs.

Table 2. Results of ANOVA and regression analysis

Objectives	R^2	R^2_{adj}	RMSE	CV errors
η	0.999	0.996	3.85×10^{-2}	8.46×10^{-2}
f_{radial}	0.998	0.993	1.58×10^{-2}	3.36×10^{-2}

RESULTS AND DISCUSSION

In a previous study, the accuracy of the numerical analysis was evaluated by validating the results of the steady flow analysis [20]. The single-channel pump model used in this validation for both the impeller and the volute was designed using the Stepanoff theory.

To carry out the multi-objective optimization of the single-channel pump volute, the RSA surrogate model was trained to construct the response surface for both of the objective functions related to the efficiency and the radial force sources. For the RSA model, both an analysis of variance (ANOVA) and a regression analysis including t-statistics [19] were conducted to measure the uncertainty in a set of coefficients in a polynomial. Table 2 shows the values for R^2 and R^2_{adj} for the second-order curve-fitting and the root mean square error (RMSE) of the RSA model. Here, R^2 and R^2_{adj} indicate the correlation coefficient in the least squares surface fitting and the adjusted correlation coefficient, respectively. As shown in Table 2, the values of R^2_{adj} for each objective function of the efficiency and radial force sources are 0.996 and 0.993, respectively. Previously, Giunta [30] suggested that the R^2_{adj} values are reliable for the $0.9 < R^2_{adj} < 1.0$ range to make an accurate prediction with the RSA models. Leave-one-out cross-validation (CV) [31] was also carried out to assess the accuracy of the RSA models. Although it is uncertain how well

the CV is correlated with the accuracy of the RSA model, the estimation of the generalization errors is nearly unbiased since it takes into account the CV of the RSA model for every design point. The CV errors that were estimated are shown in Table 2. The functional forms for both objective function values from the RSA model can be expressed in terms of normalized design variables as follows.

$$\eta = -83.4814+4.5637x_1+1.2075x_2-0.1356x_1x_2 -2.9588x_1^2-1.3024x_2^2 \quad (15)$$

$$f_{radial} = 0.6752-0.4451x_1-1.1649x_2+0.3797x_1x_2 +0.669x_1^2-0.9565x_2^2 \quad (16)$$

A hybrid MOEA based on the response surface constructed from the above RSA was employed to obtain the global POSs through using the real-coded NSGA-II. The real-coded NSGA-II was invoked to obtain well-spread, approximate POSs with 250 generations and 100 populations. The crossover and mutation probabilities were set to 0.75 and 0.5, respectively, and their parameters were set to 10 and 50, respectively. These parameters were adjusted one-by-one to suit the nature of the problem.

Figure 7 shows the global POSs that were generated by the hybrid MOEA by using the objective function values of the reference design and the design points genarated by LHS. The objective function values for the efficiency and the radial force are to be maximized and minimized. As a result, a trade-off analysis shows an obvious correlation between the efficiency and the radial force. In other words, any improvement in one objective function leads to the deterioration in the other objective function, which shows the competing nature of the two objective functions. Specifically, a lower efficiency was obtained at a lower radial force, and vice versa, for the global POSs while the difference between the maximum and minimum efficiencies among the global POSs was only ~1% (Fig. 7). Efficient designs are noted to have a lower radial force source without a major impact on the efficiency. The trade-off analysis of the global POSs therefore allows a designer to select any economic solution according to the required design conditions.

In this work, the arbitrary optimum design (AOD) extracted near the end of the global POSs, which exhibits the best performance in terms of the radial force source, was selected to find the main factors responsible for improving the performance. Since the impeller was already optimized in previous work to improve the hydraulic efficiency [24], the present study focused more on the radial force-oriented design to reduce the radial force sources due to the impeller-volute interaction resulting from the variation in the volute shape. Actually, the most important cause of faults in single-channel pumps is still the balancing problem related to vibration.

Table 3 lists the results of the multi-objective optimization of the design variables and the objective function values of the AOD, along with those for the reference design. Here, the value for f_{radial} was normalized according to the value of the reference design. Among the design variables for the AOD, CP1 changed significantly relative to the reference values [Table 3(a)]. Table 3(b) shows that the AOD has objective function values that are considerably improved realative to those of the reference design. Consequently, the AOD obtained through multi-objective optimization shows improvements of 1.58% and 0.718 in the efficiency and radial force source, respectively, relative to the reference design. On the other hand, the maximum relative errors of the hybrid MOEA predictions for the objective functions are 0.12% and 0.022, respectively. Thus, these results indicate that quite accurate predictions were obtained from the regression analysis by the MOEA coupled with a surrogate model.

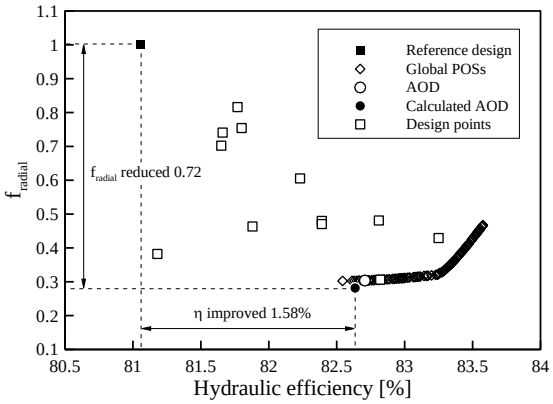

Figure 7. Global Pareto-optimal solutions

Table 3. Results of the multi-objective optimization

(a) Design variables

Designs	CP1, mm^2	CP2, mm^2
Reference design	2,000	4,000
AOD	409	4,368

(b) Objective functions

Designs	MOEA		(U)RANS		Increment	
	η, %	f_{radial}	η, %	f_{radial}	η, %	f_{radial}
Reference design	-	-	81.06	1.000	-	-
AOD	82.76	0.304	82.64	0.282	1.58	0.718

Figure 8 compares the distribution of the cross-section of the internal flow for the AOD against the reference design that has a straight distribution of the cross-sectional area. For the AOD, the theta angle shows that the cross-sectional area of the internal flow increased smoothly by making significant changes to CP1. These results indicate that the range of the theta angle from 0 to 150° that depends on CP1 has a significant effect on both objective functions.

Figure 9 shows the distribution of the unsteady radial

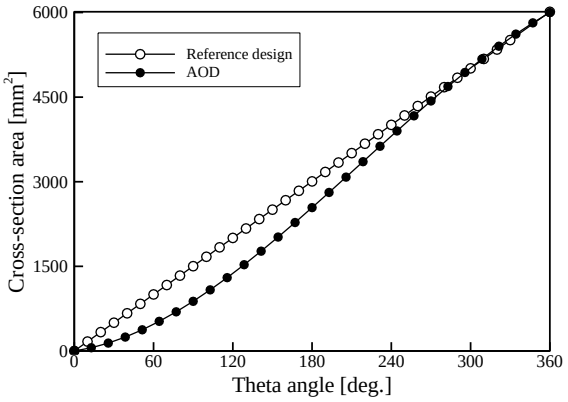

Figure 8. Comparison of the distribution of the cross-sectional area of the internal flow

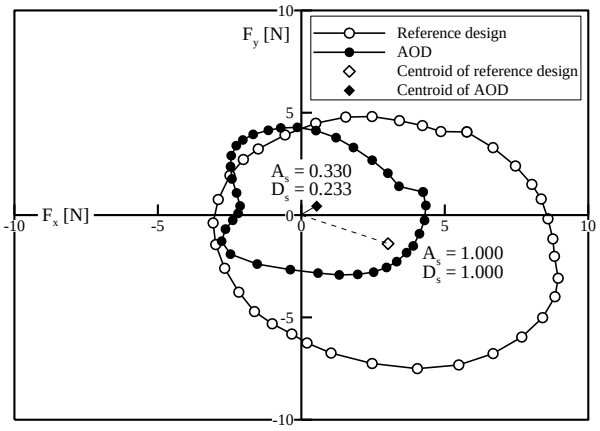

Figure 9. Unsteady radial force sources during one revolution

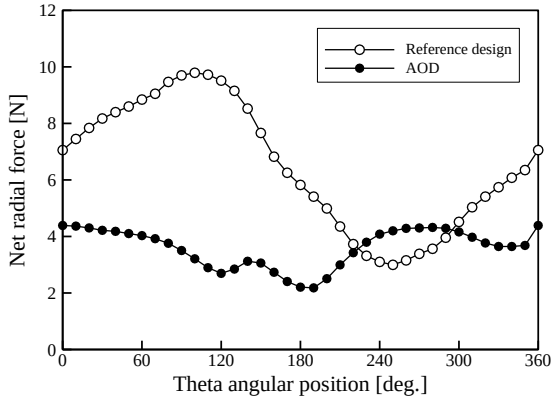

Figure 10. Unsteady net radial force fluctuation during one revolution

force sources for one revolution in the unsteady analysis. The sweep area constructed from the unsteady radial force sources of the reference design leaned toward the four quadrant direction from the origin while the AOD formed near the origin. Furthermore, the sweep area of the AOD remarkably decreased relative to the reference design. As a consequence, the sweep area and the distance for the AOD decreased by 0.670 and 0.767, respectively, relative to the reference design (Fig. 9).

Figure 10 shows the unsteady fluctuation of the net radial forces for the reference design and the AOD during one revolution. As shown in Fig. 10, the amplitude values of the fluctuation of the net radial forces of the AOD decreased significantly for most of the theta angle positions, especially in the region with a theta angle of 100°. These results highlight the considerable decrease in the radial force sources in the single-channel pump resulting from the multi-objective optimization.

Figure 11 shows the time history of instantaneous unsteady pressure contours at the boundary surface near the impeller outlet both for the reference design and the AOD. Both of the instantaneous unsteady pressure contours were compared in one rotation of the impeller. One rotation was divided into six time steps to clarify the change in the flow structure, and in both models, the bacilliform low pressure and the annular high pressure zones formed in the region of the small cross-sectional area between 0 and 70 degrees of the impeller, shown in Fig. 1, and the leading edge of the impeller, respectively.

However, the low pressure in the AOD was substantially alleviated relative to that of the reference design. In the reference design, a high pressure zone occurred on the boundary surface near the impeller outlet [Fig. 11(b)], and the large high pressure zone caused by the impeller-volute interaction increasingly developed [Fig. 11(c)]. Consequently, the imbalance with vibration caused by the non-uniform radial force arose in the entire annulus passage area of the pump. In general, the pressure distribution in the AOD is more uniform than that in the reference design, and the large high-pressure zone caused by the impeller-volute interaction is obviously suppressed (Fig. 11). As a result, the AOD produced mostly stable flows in the entire annulus passage area of the pump.

CONCLUSIONS

A single-channel pump for wastewater treatment was optimized using a hybrid MOEA and RSA surrogate model with three-dimensional steady and unsteady RANS analyses. Multi-objective optimization was conducted to simultaneously improve the efficiency and reduce the radial force sources by using two design variables related to the cross-sectional area of the internal flow of the volute. The three objective functions represented the total efficiency, the sweep area of radial force during one revolution, and the distance of the mass center of sweep area from the origin. Multi-objective optimization was used to obtain the global POSs, and the AOD with the best performance in terms of the radial force source in the POSs was selected to find the main factors responsible for the improvement in performance.

The results of the AOD showed an improvement of 1.58% in efficiency and a 0.718 decrease in the radial force sources relative to those of the reference design. Consequentially, the sweep area of the radial force during one revolution and the distance of the mass center of the sweep area from the origin decreased considerably as 0.670 and 0.767, respectively, when compared to those of the

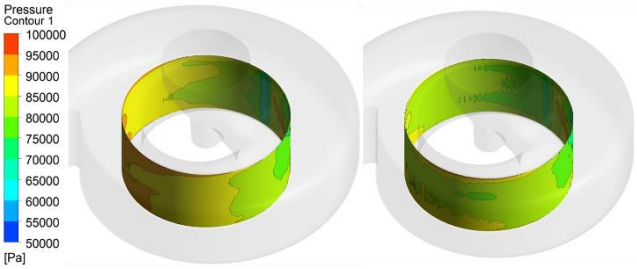

(a) T=1/6τ

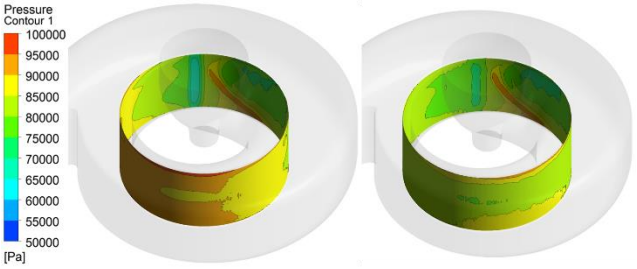

(b) T=2/6τ

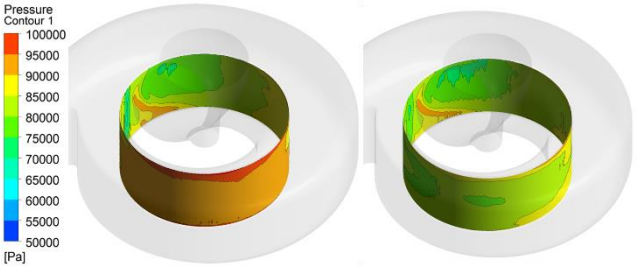

(c) T=3/6τ

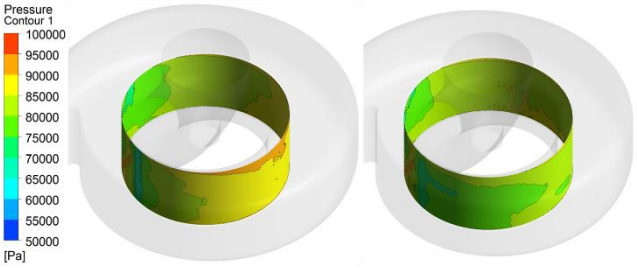

(d) T=4/6τ

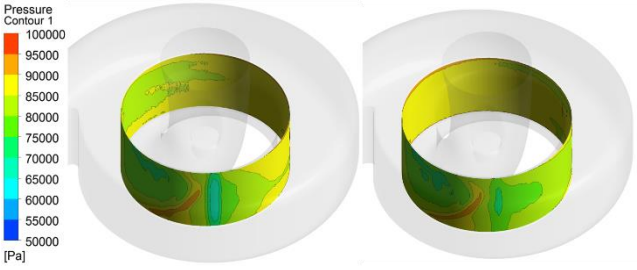

(e) T=5/6τ

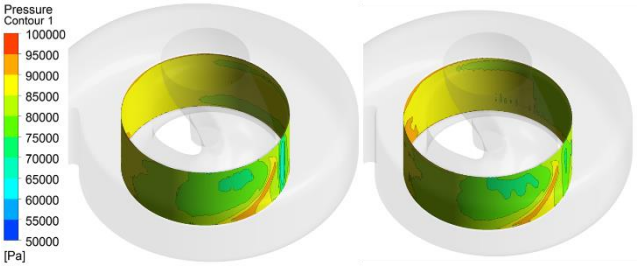

(f) T=6/6τ

Figure 11. Unsteady pressure contours

reference design. The unsteady pressure contour analyses at the boundary surface near the pump impeller outlet show that in the reference design, the high-pressure zone occurred in the wide region and that this large high-pressure zone caused by the impeller-volute interaction increasingly developed.

These results indicate that the imbalance caused by the non-uniform radial force arose throughout the entire annulus passage area of the pump. However, the pressure distribution in the AOD was generally uniform, and the large high-pressure zone caused by the impeller-volute interaction was obviously suppressed when compared to that of the reference design. This can be seen to have contributed to the decrease in the imbalance resulting from the non-uniform radial force with a simultaneous improvement in efficiency.

ACKNOWLEDGMENTS

This work was supported by a grant from the Global Hidden Champion Research Project Grant of the Korea Institute of Industrial Technology (KITECH), funded by the Korean government (MSIP) (No. JG150013). The authors gratefully acknowledge this support.

REFERENCES

[1] B. F. Hansen and P. J. Henning. Waste water pump. U.S. Patent Application. 13(886): 479, 2013.

[2] J. Pei, F. K. Benra, H. J. Dohmen. Application of different strategies of partitioned fluid–structure interaction simulation for a single-blade pump impeller. *Proceedings of the Institution of Mechanical Engineers, Part E: Journal of Process Mechanical Engineering*. 226(4): 297-308, 2012.

[3] J. Keays and C. Meskell. A study of the behavior of a single-bladed waste-water pump. *Proceedings of the Institution of Mechanical Engineers, Part E: Journal of Process Mechanical Engineering*. 220(2): 79-87, 2006.

[4] J. F. Gulich. Centrifugal pumps. Second edition, Springer, Verlag Berlin Heidelberg, 2008.

[5] J. Gonzalez, J. Fernandez, E. Blanco and C. Santolaria. Numerical simulation of the dynamic effects due to impeller-volute interaction in a centrifugal pump. *Transactions of the ASME–Journal of Fluids Engineering*. 124: 348-355, 2002.

[6] J. Gonzalez, J. Parrondo, C. Santolaria and E. Blanco. Steady and unsteady radial forces for a centrifugal pump with impeller to tongue gap variation. *Transactions of the ASME–Journal of Fluids Engineering*. 128: 454-462, 2006.

[7] D. O. Baun, L. Kostner and R. D. Flack. Effect of relative impeller-to-volute position on hydraulic efficiency and static radial force distribution in a circular volute centrifugal pump. *Transactions of the ASME–Journal of Fluids Engineering*. 121: 598-605, 2000.

[8] J. Kurokawa, T. Fujii, J. Matsui and T. Kitahora. Experimental determinations of flow characteristics in double volute. The Fifth Asian International

Conference on Fluid Machinery. Seoul, Korea, 825-832, 1997.

[9] J. Wei, L. Guojun, L. Pengfei. Z. Lisheng and Q. Hongyang. Numerical research of the effect of the outlet diameter of diffuser on the performance and the radial dorce in a single-stage centrifugal pump. Joint US-European Fluids Engineering Division Summer Meeting. Chicago, Illinois, US, FEDSM2014-21299.

[10] K. A. Kaupert and T. Staubli. The unsteady pressure field in a high specific speed centrifugal pump impeller-part I: influence of the volute. *Transactions of the ASME–Journal of Fluids Engineering*. 121: 621-626, 1999.

[11] D. O. Baun and R. D. Flack. Effects of volute design and number of impeller blades on lateral impeller forces and hydraulic performance. *International Journal of Rotating Machinery*, 9(2): 145-152, 2003.

[12] H. Alemi, S. A. Nourbakhsh, M. Raisee and A. F. Najafi. Effects of volute curvature on performance of a low specific-speed centrifugal pump at design and off-design conditions. *Journal of turbomachinery*, 137: 041009-01-10, 2015.

[13] K. Deb. Multi-objective optimization using evolutionary algorithms, 1st ed., John Wiley & Sons Inc., Chichester, England, 2001.

[14] J. H. Kim, B. Ovgor, K. H. Cha, J. H. Kim, S. Lee and K. Y. Kim. Optimization of the aerodynamic and aeroacoustic performance of an axial-flow fan. AIAA Journal, 52(9): 2032-2044, 2014.

[15] X. D. Wang, C. Hirsch, S. Kang and C. Lacor. Multi-objective optimization of turbomachinery using improved NSGA-II and approximation model. Computer Methods in Applied Mechanics and Engineering, 200(9-12): 883-895, 2011.

[16] J. H. Kim, R. Kasahara, T. Kanemoto, T. Miyaji, Y. S. Choi, J. H. Kim, K. Y. Lee and A. M. Galal. Multiobjective optimization of a counterrotating type pump-turbine unit operated at turbine mode. Advances in Mechanical Engineering, 2014: 1-11, 2014.

[17] O. Oksuz and I. S. Akmandor. Axial turbine blade aerodynamic optimization using a novel multi-level genetic algorithm. Proceedings of the ASME turbo expo 2008, Berlin, Germany, GT2008-50519, 2008.

[18] T. Goel, R. Vaidyanathan, R. T. Haftka, W. Shyy, N. V. Queipo and K. Tucker. Response surface approximation of Pareto optimal front in multi-objective optimization. *Computer Methods in Applied Mechanics and Engineering*, 196(4-6): 879-893, 2007.

[19] R. H. Myers and D. C. Montgomery. Response surface methodology-process and product optimization using designed experiments. John Wiley & Sons, Inc: New York, 1995.

[20] J. H. Kim, B. M. Cho, Y. S. Kim, Y. S. Choi, K. Y. Kim, J. H. Kim and Y. Cho. Optimization of a single-channel pump impeller for wastewater treatment. *Proceedings of The Institution of Mechanical Engineers, Part E-Journal of Process Mechanical Engineering*, in process.

[21] ANSYS Inc. ANSYS CFX-Solver Theory Guide. ANSYS CFX-11.0, 2006.

[22] F. R. Menter. Two-equation eddy-viscosity turbulence models for engineering application. *AIAA Journal*, 32(8): 1598–1605, 1994.

[23] J. E. Bardina, P. G. Huang and T. J. Coakley. Turbulence modeling validation 28th AIAA Fluid Dynamics Conference, AIAAPaper 1997-2121, June–July 1997.

[24] B. M. Cho, J. H. Kim, Y. S. Choi, J. W. Kim, Y. S. Kim, T. S. Ahn, J. H. Kim. Surrogate based optimization of a single-channel pump impeller. 7th International Conference on Pumps and Fans 2015 (ICPF 2015), October 18-21, 2015, Hangzhou, Zhejiang Province, China, ICPF-121, to be presented.

[25] J. Sacks, W. J. Welch, T. J. Mitchell and H. P. Wynn. Design and analysis of computer experiments. *Statistical Science*, 4(4): 409–435, 1989.

[26] MATLAB, The language of technical computing, software package, Release 14, THE MATHWORKS INC., Natick, MA, 2004.

[27] E. Benini. Three-dimensional multi-objective design optimization of a transonic compressor rotor. *Journal of Propulsion and Power*, 20(3): 559-565, 2004.

[28] J. H. Kim J. W. Kim and K. Y. Kim. Axial-flow ventilation fan design through multi-objective optimization to enhance aerodynamic performance. *Journal of Fluids Engineering - Transactions of The ASME*, 133(10): Paper 101101, 2011.

[29] Y. Lian and M. S. Liou. Multiobjective optimization using coupled response surface model and evolutionary algorithm. *AIAA Journal*, 43(6): 1316–1325, 2005.

[30] A. A. Giunta. Aircraft multidisciplinary design optimization using design of experimental theory and response surface modeling methods. Ph.D. thesis, Department of Aerospace Engineering, Virginia Polytechnic Instituteand State University, Blacksburg, VA, 1997.

[31] N. V. Queipo, R. T. Haftka, W. Shyy, T. Goel, R. Vaidyanathan and P. K. Tucker. Surrogate-based analysis and optimization. *Progress in Aerospace Sciences*, 41(1): 1–28, 2005.